

Hybrid RIS-assisted interference mitigation for heterogeneous networks

Abdel Nasser Soumana Hamadou¹, Ciira wa Maina², Moussa Moindze Soidridine³

¹Department of Electrical Engineering, Pan African University Institute for Basic Sciences, Technology and Innovation (PAUSTI), Nairobi, Kenya

²Centre for Data Science and Artificial Intelligence (DSAIL), Dedan Kimathi University of Technology (DeKUT), Nyeri, Kenya

³Faculty of Science and Techniques, UAMA University, Dakar, Senegal

Article Info

Article history:

Received Jan 14, 2024

Revised Mar 5, 2024

Accepted Mar 25, 2024

Keywords:

Co-tier interference
Cross-tier interference
Energy efficiency
HetNet
Hybrid RIS
Spectral efficiency
RIS

ABSTRACT

Reconfigurable intelligent surfaces (RIS) have evolved as a low-cost and energy-efficient option to increase wireless communication capacity. In this research, we suggest using hybrid RIS (H-RIS) to reduce interference in heterogeneous networks (HetNet). In contrast to traditional passive RIS, a hybrid RIS is suggested, which is fitted with a few active elements to not only reflect but also amplify incident signals for a significant performance increase. By jointly optimising the passive and active coefficients of the H-RIS, we aim to maximise the rate of the small cell user (SUE). We presented an effective alternating optimisation (AO)-based phase shift matrix coefficients (AO-PMC) technique to tackle this problem by iteratively optimising these variables because the optimisation problem is not convex. The simulation results demonstrate that, in comparison to the passive RIS-assisted HetNet scheme and the scheme without RIS, the suggested scheme, with just 8% of active elements, can enable HetNet to gain superior spectral efficiency (SE) and energy efficiency (EE). The outcomes also demonstrate that, in the majority of the cases taken into account, H-RIS can outperform the active RIS-assisted HetNet scheme.

This is an open access article under the [CC BY-SA](https://creativecommons.org/licenses/by-sa/4.0/) license.



Corresponding Author:

Abdel Nasser Soumana Hamadou

Department of Electrical Engineering, Pan African University Institute for Basic Sciences

Technology and Innovation (PAUSTI)

Nairobi, Kenya

Email: nasser.abdel@students.jkuat.ac.ke

1. INTRODUCTION

Reconfigurable intelligent surfaces (RIS), which may optimise the wireless environment by fine-tuning the phase shifts of numerous inexpensive passive elements, have garnered a lot of interest from the wireless communication community [1]-[6]. RIS has been used in a number of wireless communication techniques, including multi-input multi-output (MIMO) systems, mobile edge computing (MEC), mmWave channels, cell-free networks, unmanned aerial vehicles (UAV), non-orthogonal multiple access (NOMA), and backscatter communication systems, due to its effectiveness in enhancing energy efficiency and spectral efficiency [1]-[4], [7]-[11]. In order to increase system capacity, spectral efficiency (SE), and network coverage by converting small cells into macro cells, a heterogeneous network, or heterogeneous networks (HetNet), is a crucial network for beyond 5G communications [12]. Furthermore, by densely deploying small cells (SC) throughout the network, HetNet may substantially boost coverage and network speed [13]. Unfortunately, despite the enormous benefits of the purposefully deployed SCs in HetNet, several obstacles occur, such

as the SCs' high-power consumption, interference between them (co-tier interference), and interference from the macrocell (cross-tier interference).

In this study, we consider the interference management problem for HetNet by deploying a hybrid RIS (H-RIS) to balance data rates and interference among various cells. We suggest using hybrid RIS, which combines active beamforming (relaying) and passive beamforming (reflecting), as opposed to conventional RIS, which can only adjust the phaseshift of the reflecting elements, or active RIS, which can also amplify the reflected signals by using additional power. As a result, the H-RIS is proven to significantly increase system spectrum efficiency, capacity, energy efficiency, and interference suppression [14]-[16].

Given the benefits of RIS mentioned above, interference control issues for RIS-assisted networks have drawn the attention of numerous academics. Xu *et al.* [12] presented a quadratic transformation method and a Lagrange dual theory method to improve the total interference efficiency of the two-tier orthogonal frequency division multiple access (OFDMA)-based HetNet in order to enhance system robustness and reduce harmful interference for macrocell users (MUs). Nonetheless, interference from macro-BS was not taken into account in the femtocell. Hybrid relay-RIS-assisted (HR-RIS) wireless communications, with a large number of passive elements and a small number of active ones, were proposed by the authors in [14]. The simulation results demonstrated that the HR-RIS-assisted system scheme outperformed the relay-assisted system scheme in terms of spectral and energy efficiency. Nonetheless, this study did not demonstrate the performance of their proposed HR-RIS in comparison to a simple active RIS scheme. In order to increase the capacity of RIS-assisted wireless networks, Chen [15] presented a new RIS design in which each RIS element can function in either an active or passive mode.

A probability-learning-based approach was presented to achieve this goal. A hybrid RIS-assisted device-to-device (D2D) application was proposed in [16] to mitigate cross-system interference. However, this study only considered the D2D network, and the energy efficiency of the system was not considered as well. For instance, to increase spectrum efficiency, Xu *et al.* [17] designed a resource allocation scheme for RIS-assisted HetNet with non-orthogonal multiple access (NOMA). But only cross-tier interference is considered.

Tan *et al.* [18] examined the end-to-end performance of RIS-assisted wireless communication. To realise this objective, they maximise the passive beamforming matrix at the RIS to achieve high SNR performance in the RIS-assisted system. However, this study did not consider MIMO systems. Zhu *et al.* [19] proposed a semidefinite programming method to relax the non-convexity of the problem and developed a low-complexity scheme to enhance the sum throughput of the RIS-assisted wireless powered heterogeneous networks (WPHN). Nevertheless, this work takes only internet of things (IoT) networks into account.

Ao *et al.* [20] investigated a resource allocation challenge for RIS-assisted D2D communication in HetNet in order to maximise the system sum rate. To achieve this goal, they optimise the resource allocation problem using game theory, the power allocation problem using the gradient descent method, and the passive beamforming matrix at the RIS using the local search method. However, this study only considers the system's rate. Moreover, in order to determine which one performs best in a typical wireless system in terms of system sum-rate, Zhang *et al.* [21] compared active RIS versus passive RIS. To increase the system sum-rate, Xu *et al.* [22] proposed a hybrid decode-and-forward (DF) relay with RIS-assisted multi-input, single-output (MISO) communication (HDF-RIS). Additionally, the data show that HDF-RIS typically had a greater sum-rate than conventional passive RIS.

Wu and Zhang [23] proposed reducing the total transmit power of a RIS-assisted single-cell wireless system by optimising both the transmit beamforming at the access point and the passive beamforming at the RIS. However, this study did not consider a multicell wireless system. Niu and Liang [24], the authors look into improving the weighted sum-rate of a multiuser MISO system assisted by a simultaneously transmitting and reflecting reconfigurable intelligent surface (STAR-RIS). To do this, they employ the element wise optimisation method to tune the transmit beamforming of the base station as well as the transmit and reflecting coefficients of the STAR-RIS. Nonetheless, only multiuser MISO systems were taken into account, and the effects of reflecting and transmitting users were not taken into account.

Ahmed *et al.* [25] provided a STAR-RIS study for several use cases in 5G and beyond networks. They classify the approaches within the domain, which include expanding coverage, improving physical security, raising sum-rate, increasing energy efficiency, and mitigating interference. The works in [14]-[16] were the exceptions, where the authors proposed a hybrid RIS to reduce interference in D2D networks, increase capacity in MIMO systems, and boost energy efficiency for a 4×2 MIMO system, respectively, without comparing the SE of the hybrid RIS over an active RIS optimised via alternating optimisation (AO) and a passive RIS

optimised via AO. Cross-tier and co-tier interference in the system was not taken into consideration. Because of that, a study of hybrid RIS-assisted interference mitigation for HetNet is necessary, especially for maximizing system SE and network performance concerning cross-tier and co-tier interference.

Therefore, this research proposes the integration of H-RIS into HetNet, which is anticipated to improve the system’s SE and EE performance and reduce interference. In addition, further research needs to be done on the issue of cross-tier and co-tier interference when H-RIS and multi-tier networks are present. As a result, in this study, we propose an H-RIS-assisted HetNet that makes use of numerous small base stations (SBS) and a macro base station (MBS) with multiple antennas, where passive and active elements can coexist. Thus, passive and active are the two ways that each H-RIS element can operate. In this regard, when the H-RIS elements correspond to the passive, the signal is reflected by the RIS elements without being amplified; however, when the H-RIS elements correspond to the active, the reflected signals are amplified by the H-RIS at the expense of additional power consumption. The main contributions are as follows:

- We develop an innovative SE and energy efficiency (EE) maximization approach for a hybrid RIS-assisted HetNet framework.
- We suggest a new methodology based on an AO framework to simultaneously determine the phase shift of all H-RIS coefficients. This framework optimises the active phase shift coefficients by converting the problem into a fractional programming (FP) problem with fixed passive phase shift coefficients, while the passive phase shift coefficients are optimised using the Dinkelbach method with fixed active phase shift coefficients.
- We study how a H-RIS aids in the resolution of cross-tier and co-tier interference concerns in HetNet.
- Finally, the suggested method is assessed using numerous numerical computations, and the results show that it outperforms passive and active RIS optimized via AO in SE and EE performance.

The rest of the paper is organised as follows: Section 2 presents the system model under consideration. The problem is then framed in section 3, the optimisation method is offered in section 4, the energy consumption model is defined in section 5, the simulation settings are shown in section 6, and the results obtained will be presented and discussed in section 7. Finally, the conclusion and future work of hybrid RIS with machine learning or the metaheuristic method are provided.

2. SYSTEM MODEL

We consider a downlink two-tier H-RIS, HetNet system, as shown in Figure 1, in which an H-RIS with N elements and a set of I small cell tiers (SC) each with a single antenna SBS are uniformly distributed and deployed to improve transmission quality between SBS_i and the U small cell user equipment (SUE) under the coverage of macro cells with M antenna MBS. The H-RIS, as opposed to traditional RIS, is made up of K active elements, $(N - K)$ passive elements and $K \ll N$.

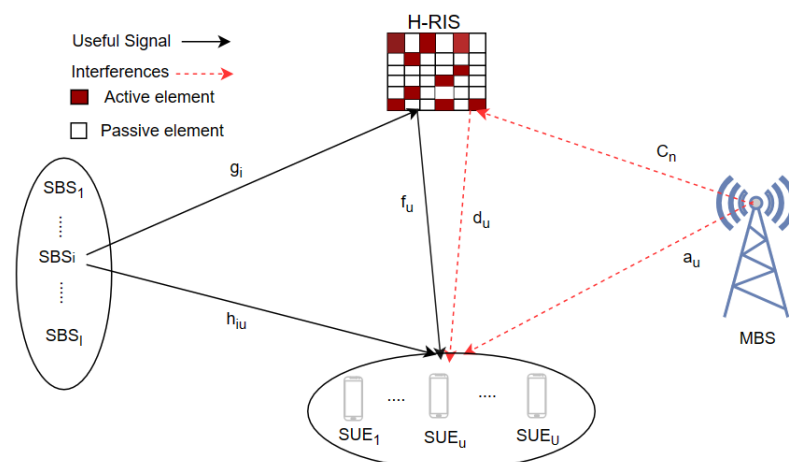


Figure 1. H-RIS-assisted HetNet scheme model

Consider that $x_i = \sqrt{P_i}s_i$ and $x_m = \sqrt{P_m}s_m$ are the transmit signals from the i^{th} SBS to the u^{th} small SUE and the MBS, respectively, and that s_i and s_m are the desired signals from the i^{th} SBS to the u^{th} SUE and the cross-tier interference from the MBS. Regarding the transmit signal from the other co-tier SBS to the u^{th} SUE of the i^{th} SBS, assuming that is $\tilde{x} = \sum_{j \neq i}^I x_j = \sum_{j \neq i}^I \sqrt{P_j}s_j$ the transmit co-tier interference to the u^{th} SUE. Consequently, we write $a_u = [a_{1u}, a_{2u}, \dots, a_{Mu}]^T \in \mathbb{C}^{M \times 1}$ to denote the channel vector between the MBS and the u^{th} SUE, and $d_u = [d_{1u}, d_{2u}, \dots, d_{Nu}]^T \in \mathbb{C}^{N \times 1}$ to denote the cascaded interference reflected channel vector from the MBS-H-RIS to the u^{th} SUE. Denoting the channel vector from the MBS to the n^{th} H-RIS element by $c_n = [c_{1n}, c_{2n}, \dots, c_{Mn}]^T \in \mathbb{C}^{M \times 1}$, the channel matrix from the M MBS antenna to the N H-RIS element is expressed as $C_{mn} \in \mathbb{C}^{M \times N}$. Denoting the channel coefficient vector between the SBS $_i$ and the u^{th} SUE, the channel vector between the SBS $_i$ and the N H-RIS element, and the channel vector between the N H-RIS element and the u^{th} SUE by $h_{iu} \in \mathbb{C}$, $g_i = [g_{i1}, g_{i2}, \dots, g_{iN}]^T \in \mathbb{C}^{N \times 1}$ respectively. As a result, the set of active elements in H-RIS is denoted by Q and the phase shift matrix for H-RIS is denoted by $A = \text{diag}(\theta_1, \theta_2, \dots, \theta_N), \theta_n$.

$$\theta_n = \begin{cases} \alpha_n e^{j\mu_n}, & \text{if } n \in Q \\ e^{j\mu_n} & \text{if } n \notin Q \end{cases} \quad (1)$$

Where α_n is the amplification factor of the signal, and it is greater than one ($\alpha_n > 1$) when the H-RIS element are active, and $\alpha_n = 1$ when the H-RIS element are passive and $\mu_n \in [0, 2\pi]$ represent the phase shift signal at the n^{th} element. In order to simplify the H-RIS circuitry, in this work, we analyse a fixed H-RIS architecture in which the number of active elements and their positions, i.e., set Q , are preset and fixed, and the amplification factor of the H-RIS element in active ways is fixed. For ease of notation, the phase shift matrix can be described as the sum of two matrices, as $A = \Phi + \Psi$, in which $\Phi = \text{diag}(\phi_1, \phi_2, \dots, \phi_N)$ and $\Psi = \text{diag}(\psi_1, \psi_2, \dots, \psi_N)$ are the phase shift matrix corresponding to the passive elements and active elements, respectively, where θ, ϕ and $\psi \in \mathbb{C}^{N \times 1}$. ϕ_n and ψ_n are written as (2) and (3).

$$\phi_n = \begin{cases} 0, & \text{if } n \in Q \\ e^{j\mu_n} & \text{if } n \notin Q \end{cases} \quad (2)$$

and,

$$\psi_n = \begin{cases} \alpha_n e^{j\mu_n}, & \text{if } n \in Q \\ 0 & \text{if } n \notin Q \end{cases} \quad (3)$$

Consequently, the received signal at the u^{th} SUE attached to the SBS $_i$ expressed be written as (4).

$$y_u = (h_{iu} + f_u^T A g_i) \sqrt{P_i} s_i + \sum_{\substack{j=1 \\ j \neq i}}^I (h_{ju} + f_u^T A g_j) \sqrt{P_j} s_j \\ + (a_u + d_u^T A c_n) \sum_{m=1}^M \sqrt{P_m} s_m + f_u^T A n_r + n_u \quad (4)$$

The desired signal of the u^{th} SUE from the i^{th} SBS is represented by the first part, the interference from other SBS by the second part, the interference from the MBS by the third part, the dynamic noise brought on by the active RIS elements by the fourth part, and the gaussian noise by the fifth part, while P_i and P_m are the transmit power from the i^{th} SBS and the MBS to the u^{th} SUE, respectively. $n_r \sim \mathcal{CN}(0, \sigma_r^2)$ is the dynamic noise introduced at the H-RIS elements in active mode and $n_u \sim \mathcal{CN}(0, \sigma_u^2)$ is the additive gaussian noise received at the u^{th} user. The H-RIS element is hence passive when $n_r = 0$ and active when $n_r \sim \mathcal{CN}(0, \sigma_r^2)$. From (4), the signal-to-interference-plus-noise ratio at the u^{th} user is expressed as (5).

$$SINR_u = \frac{|h_i|^2 P_i}{\sum_{j \neq i}^I |h_j|^2 P_j + |h_n|^2 \sum_{m=1}^M P_m + \|f_u^T A\|^2 \sigma_r^2 + \sigma_u^2} \quad (5)$$

Where $h_i = h_{iu} + f_u^T A g_i$ is the channel from the i^{th} SBS to the u^{th} user, which includes both direct link and reflected link, and $h_n = a_u + d_u^T A c_n \in \mathbb{C}^{1 \times M}$. Therefore, based on (5), the achievable rate at the u^{th} SUE is represented as (6).

$$R_u = \log_2 (1 + SINR_u) \tag{6}$$

3. FORMULATION OF THE PROBLEM

Our goal in this work is to maximise the rate of the H-RIS-assisted HetNet system. In light of this, we concentrate on the problem of optimising the phase shift matrix A, which is denoted by (7).

$$\begin{aligned} \max_A \quad & R_u \\ \text{s.t.} \quad & |\theta_n| = 1; \text{ for } n \notin Q \\ & |\theta_n \sigma_r^2|^2 + |\theta_n g_i|^2 P_i \leq P_{RIS}^{max}; \text{ for } n \in Q \end{aligned} \tag{7}$$

Where P_{RIS}^{max} is the power budget of the H-RIS active elements. Directly solving problem (7) is challenging due to the fact that it is not convex with regard to ϕ and ψ . As a result, in the section that follow, we optimise ϕ and ψ individually using the AO method.

4. METHOD

The methodology was developed to improve the previous results [7]. In order to address the problems with the joint active phase shift matrix and passive phase shift matrix in this part, we use a method of AO that alternately optimises ϕ and ψ . The method steps used in this study are illustrated in Algorithm 1.

4.1. Proposed AO-based phase shift matrix coefficient (AO-PMC) method

For the sake of simplicity, let B symbolise the following diagonal matrix:

$$[B]_N^Q = \begin{cases} 1, & \text{for } n \in Q \\ 0 & \text{for } n \notin Q \end{cases} \tag{8}$$

and define $[B]_N^{\bar{Q}} = [B]_N - [B]_N^Q$, therefore we have $\phi = [B]_N^{\bar{Q}} \theta = [B]_N^{\bar{Q}} \phi$ and $\psi = [B]_N^Q \theta = [B]_N^Q \psi$. Following that, we solve the ϕ and ψ problems, respectively.

4.1.1. Using a fixed ψ to optimise ϕ

Let us define the following variables when ψ is fixed:

$$\begin{aligned} Z &= \text{diag} \left(f_u^T \right) g_i & h_1 &= Z^T \psi + h_{iu} \\ \Omega &= \text{diag} \left(d_u^T \right) c_n & h_3 &= \Omega \psi^T + a_u \\ \alpha &= \text{diag} \left(f_u^T \right) \sigma_r^2 & \bar{Z} &= [B]_N^{\bar{Q}} Z \\ \sigma_T^2 &= \psi^T \alpha \alpha^T \psi + \sigma_u^2 & \text{and } \bar{\Omega} &= [B]_N^{\bar{Q}} \Omega \end{aligned} \tag{9}$$

then, the optimisation problem of ϕ can be represented as (10).

$$\begin{aligned} \max_{\phi} \quad & \log_2 \left(1 + \frac{P_i |\bar{Z}^T \phi + h_1|^2}{\sum_{\substack{j=1 \\ j \neq i}}^I |\bar{Z}^T \phi + h_1^T|^2 P_j + |\bar{\Omega}^T \phi + h_3^T|^2 \sum_{m=1}^M P_m + \sigma_T^2} \right) \\ \text{s.t.} \quad & \phi = [B]_N^{\bar{Q}} \phi \\ & |\phi_n| = 1; n = 1, \dots, N \end{aligned} \tag{10}$$

Due to the proportionality between the problem (10) and its SINR, we have a (11).

$$\max_{\phi} \log_2(1 + SINR_u(\phi)) \iff \max_{\phi} SINR_u(\phi) \quad (11)$$

Because of this, we may remove the logarithmic operation, which transforms problem (10) into a nonlinear fractional programming problem. On the basis of the Dinkelbach approach [26], letting,

$$f(\phi) = P_i |\bar{Z}^T \phi + h_1|^2 - \lambda (I_j + I_m + \sigma_T^2) \quad (12)$$

where $I_j = \sum_{j=1}^I |\bar{Z}^T \phi + h_1|^2 P_j$, $I_m = |\bar{\Omega}^T \phi + h_3|^2 \sum_{m=1}^M P_m$, and λ is an auxiliary variable, and $f(\phi)$ is the objective function in problem (10). Consequently, the problem (10) can be reformulated as (13).

$$\begin{aligned} \max_{\phi} \quad & f(\phi) \\ \text{s.t.} \quad & |\phi_n| = 1; n = 1, \dots, N \end{aligned} \quad (13)$$

Problem (13) becomes easier to solve if we set λ to 0. This implies that $f(\phi) = P_i |\bar{Z}^T \phi + h_1|^2$, because $\phi = [\phi_1, \phi_2, \dots, \phi_N]^T$, problem (13) can be modeled as (14).

$$\begin{aligned} \max_{\phi} \quad & \phi^T \bar{Z} \bar{Z}^T \phi + \phi^T \bar{Z} h_1 + h_1 \bar{Z}^T \phi + \|h_1\|^2 \\ \text{s.t.} \quad & |\phi_n| = 1; n = 1, \dots, N \end{aligned} \quad (14)$$

Because the objective function of problem (15) contains quadratic terms of ϕ and problem (15) has only a unit-modular constraint, it can be solved using the semi-definite relaxation (SDR) method [27], [28]. Then, by setting,

$$W = \begin{bmatrix} \phi \\ 1 \end{bmatrix} \begin{bmatrix} \phi^T & 1 \end{bmatrix} \quad (15)$$

and:

$$L = \begin{bmatrix} \bar{Z} \bar{Z}^T & \bar{Z} h_1 \\ h_1 \bar{Z}^T & 0 \end{bmatrix} \quad (16)$$

the optimisation can therefore be simplified to (17).

$$\begin{aligned} \max_{\phi} \quad & \phi^T L \phi + \|h_1\|^2 \\ \text{s.t.} \quad & |\phi_n| = 1; n = 1, \dots, N \end{aligned} \quad (17)$$

Additionally, problem (17) is still non convex because the rank-one constraint is not convex and W needs to be satisfied by $rank(W) = 1$ and $W \succeq 0$. It can be eliminated first to create a more relaxed optimisation problem, as in (18).

$$\begin{aligned} \max_W \quad & trace(LW) + \|h_1\|^2 \\ \text{s.t.} \quad & W_{n,n} = 1; n = 1, \dots, N \\ & W \succeq 0 \end{aligned} \quad (18)$$

Utilizing a convex optimisation tool like CVX [29] can help address this convex optimisation problem. In order to determine the rank-one solution, the gaussian randomization approach can then be used. The following are the precise steps for ϕ optimisation: the iteration index $l = 0$ is first set. We then find (17) for $\lambda = 0$. Then, in order to meet the rank-one criteria and yield ϕ , we create W using gaussian randomization method. $\lambda^* = \frac{|\bar{Z} \phi + h_1|^2}{(I_j + I_m + \sigma_T^2)}$ is then computed using Dinkelbach technique, and if $f(\phi) < 10^{-6}$ is satisfied, return $\phi = \phi^*$; otherwise, set $\lambda(l+1) = \lambda^*$ and $l = l+1$.

4.1.2. Using a fixed ϕ to optimise ψ

Now that we have the target problem defined, we can move on to solving it by maximising ψ with a fixed ϕ . To do this, we define the following variables to make the target problem formulation simpler.

$$\begin{aligned} \bar{h}_1 &= Z^T \phi + h_{iu} & \bar{h}_3 &= \Omega \phi^T + a_u \\ \tilde{Z} &= [B]_N^Q Z & \alpha_1 &= \alpha [B]_N^Q \\ \tilde{\Omega} &= [B]_N^Q \Omega & \bar{h} &= \tilde{Z}^T \psi + \bar{h}_1 \\ \text{and } \bar{h}_2 &= \tilde{\Omega}^T \psi + \bar{h}_3 \end{aligned} \tag{19}$$

The objective function of ψ is then represented as (20).

$$f(\psi) = \log_2 \left(1 + \frac{P_i |\bar{h}|^2}{\sum_{\substack{j=1 \\ j \neq i}}^I |\bar{h}|^2 P_j + |\bar{h}_2|^2 \sum_{m=1}^M P_m + |\alpha_1 \psi|^2 + \sigma_u^2} \right) \tag{20}$$

Regarding the power constraint, by setting in (21).

$$\begin{aligned} P_R &= \psi^T \left(\text{diag}(g_i P_i) (\text{diag}(g_i P_i))^T + \sigma_r^2 [B]_N^Q \right) \psi \\ &= \psi^T \bar{D} \psi \end{aligned} \tag{21}$$

Where $\bar{D} = [B]_N^Q D [B]_N^Q$ and $D = \left(\text{diag}(g_i P_i) (\text{diag}(g_i P_i))^T + \sigma_r^2 [B]_N^Q \right)$. As a result, the ψ optimisation is denoted as (22).

$$\begin{aligned} \max_{\psi} & f(\psi) \\ \text{s.t. } & \psi = [B]_N^Q \psi \\ & \psi^T \bar{D} \psi \leq P_{RIS}^{max} \end{aligned} \tag{22}$$

We use the fractional programming techniques suggested in [30] to convert the problem (22) into quadratic form in order to handle the non-convex logarithms and fractions. This leads to the following: by introducing auxiliary variables $\bar{C} = [\bar{c}_1, \bar{c}_2, \dots, \bar{c}_N] \in \mathbb{R}^N, \forall_n \in Q$ and $Y = [y_1, y_2, \dots, y_N] \in \mathbb{C}^N, \forall_n \in Q$, the problem (22) is then transformed as (23).

$$\begin{aligned} \max_{\psi} & f(\psi, \bar{C}, Y) = \log(1 + \bar{C}) - \bar{C} + g(\psi, \bar{C}, Y) \\ \text{s.t. } & \psi^T \bar{D} \psi \leq P_{RIS}^{max} \end{aligned} \tag{23}$$

Where $g(\psi, \bar{C}, Y)$ is defined as (24).

$$g(\psi, \bar{C}, Y) = 2P_i \sqrt{1 + \bar{C}} \text{Re}\{ \bar{h} Y \} - |Y|^2 \left(\sum_{\substack{j=1 \\ j \neq i}}^I |\bar{h}|^2 P_j + |\bar{h}_2|^2 \sum_{m=1}^M P_m + |\alpha_1 \psi|^2 + \sigma_u^2 \right) \tag{24}$$

With fixing Y and ψ , the optimal \bar{C} can be obtained by solving $\frac{\partial f(\psi, \bar{C}, Y)}{\partial \bar{C}} = 0$ as (25).

$$\bar{c}_n^{opt} = \frac{P_i \text{Re}\{ \bar{h} Y^{opt} \} - P_i \text{Re}\{ \bar{h} Y^{opt} \} \sqrt{P_i \text{Re}\{ \bar{h} Y^{opt} \} + 4}}{2} \tag{25}$$

After fixing the auxiliary variable \bar{C} and the active phase matrix ψ , the optimal Y can be derived by solving $\frac{\partial f(\psi, \bar{C}, Y)}{\partial Y} = 0$, which is given as (26).

$$y_n^{opt} = \frac{\sqrt{1 + \bar{C}h}P_i}{\sum_{j \neq i}^I |\bar{h}|^2 P_j + \sum_{m=1}^M |\bar{h}_2|^2 P_m + |\alpha_1 \psi|^2 + \sigma_u^2} \quad (26)$$

Using \bar{h} , \bar{h}_2 and fixing the auxiliary variables \bar{C} and Y the problem (23) can be rewritten as (27).

$$\begin{aligned} \max_{\psi} \quad & \text{Re} \{2\psi^T S\} - \psi^T H \psi \\ \text{s.t.} \quad & \psi^T \bar{D} \psi \leq P_{RIS}^{max} \end{aligned} \quad (27)$$

Where,

$$S = P_i \sqrt{1 + \bar{c}_n^{opt}} \tilde{Z} y_n^{opt} - |y_n^{opt}|^2 \tilde{Z} h_1 \sum_{\substack{j=1 \\ j \neq i}}^I P_j \quad (28)$$

and,

$$\begin{aligned} H = & |y_n^{opt}|^2 \alpha_1 \text{diag}(f_u) \sigma_u^2 + |y_n^{opt}|^2 \sum_{\substack{j=1 \\ j \neq i}}^I P_j \tilde{Z} \text{diag}(f_u) \\ & + |y_n^{opt}|^2 \sum_m^M P_m \tilde{Z} \text{diag}(d_u) \end{aligned} \quad (29)$$

It is noted that problem (27) is a standard quadratically constrained quadratic programme (QCQP) problem that may also be solved using Lagrange multiplier approach. Given $\bar{\mu}$ as Lagrange multiplier, the Lagrangian is (30).

$$\mathcal{L}(\psi, \bar{\mu}) = \psi^T H \psi - \text{Re} \{2\psi^T S\} + \bar{\mu} (\psi^T \bar{D} \psi - P_{RIS}^{max}) \quad (30)$$

Thus the optimal value of ψ is (31).

$$\psi^{opt} = \frac{S}{H + \bar{\mu} \bar{D}} \quad (31)$$

The optimal $\bar{\mu}$ is the solution to the following problem in (32).

$$\begin{aligned} \max_{\bar{\mu}} \quad & -S^T (H + \bar{\mu} \bar{D})^{-1} S - \bar{\mu} P_{RIS}^{max} \\ \text{s.t.} \quad & \bar{\mu} > 0 \end{aligned} \quad (32)$$

A one-dimensional search methods can be used to find the optimal $\bar{\mu}$. Additionally, the specific steps for optimizing ψ with ϕ are provided in Algorithm 1.

Algorithm 1 Proposed AO-PMC

Input: initialize ϕ^0 , ψ^0 compute A^0 set $l = 0$, convergence accuracy ϵ , $\bar{\mu} = 0$, $\lambda = 0$, R_u^0 .

Repeat

1 : $l = l + 1$

2: Update λ by $\lambda^* = \frac{|\bar{Z}\phi + h_1^T|^2}{(I_j + I_m + \sigma_T^2)}$

3: Update ϕ by (18)

4: Update \bar{C} by (25)

5: Update Y by (26)

6: Update S by (28)

7: Update H by (29)

8: Update $\bar{\mu}$ by (32)

9: Update ψ by (31)

Until : $R_u^l - R_u^{l-1} < \epsilon$.

Output $A = \phi^l + \psi^l$

5. MODEL OF ENERGY CONSUMPTION

5.1. Without RIS (No-RIS) scheme

With the without RIS method, we simulate the network without deploying any RIS, allowing us to model the network's total power consumption as [1], [31].

$$P_{w/O} = \frac{P_i}{\tau} + P_{SUE,u} + P_{SBS} \quad (33)$$

Where τ is the power amplifier efficiency and $P_{SUE,u}$ is the hardware static power dissipation by the u^{th} user equipment, while P_{SBS} and P_i denote the total hardware static power consumption at the SBS and the SBS transmit power at the u^{th} user equipment, respectively.

5.2. Passive RIS scheme

The total power consumption of the proposed H-RIS-assisted HetNet system is compared to that of the passive RIS-assisted HetNet system. We can see that there is no active element in the latter, but $N=M+K$ passive elements are used at the RIS. As a result, the overall power consumption of the RIS-assisted HetNet system can be stated as [1], [14], [15], [28].

$$P_{RIS} = \frac{P_i}{\tau} + P_{SUE,u} + P_{SBS} + NP_b \quad (34)$$

Where P_b is the power required for one RIS element [14], [15].

5.3. Active RIS scheme

The total power consumption of the active RIS-assisted HetNet system is then contrasted with that of the proposed H-RIS-assisted HetNet system. We observe that in this case, a passive element is absent, while the RIS makes use of active elements. Consequently, the total energy used by the active RIS-assisted HetNet system can be modeled as [1], [14], [15], [28].

$$P_{Active} = \frac{P_i}{\tau} + P_{SUE,u} + P_{SBS} + NP_a + \frac{P_A}{\tau} \quad (35)$$

Where $P_A = |\theta_n \sigma_r^2|^2 + |\theta_n g_i|^2 P_i$ is the amplification power of the active RIS element, and P_a is the power required by one active RIS element.

5.4. H-RIS scheme

The number of active and passive elements in the H-RIS scheme is fixed at K and M , respectively. In light of this, the total power consumption of the HetNet system, aided by H-RIS, can be expressed as [1], [14], [15], [28].

$$P_H = \frac{P_i}{\tau} + P_{SUE,u} + P_{SBS} + MP_b + K(P_a - P_b) + \frac{P_A}{\tau} + NP_{SW} \quad (36)$$

Where the last terms accounts for the total power consumed by the N mode shifts in the RIS elements, each demands a power of P_{SW} . Then, the EE of a scheme is given as (37).

$$EE = \frac{\log_2(1 + SINR_u)}{P} \text{ (bits/J/Hz)} \quad (37)$$

Where P is the total power consumption and is given by (33), (34), (35), and (36) for each scheme.

6. SIMULATION SETTINGS

The i^{th} SBS is at a distance of $(50(i - 1), 0)$ where $i \in (1, 2, 3, 4)$, the u^{th} SUE is at a distance of 65m [17] form the origin point $(0, 0)$, where its coordinate are $(x_{SUE,u}, y_{SUE,u})$, where $x_{SUE,u}$ is the distance between the i^{th} SBS and the u^{th} SUE, and the H-RIS is located at a distance of 70m [17] form the origin point $(0, 0)$, where the distance between the i^{th} SBS and the H-RIS is x_t ; thus, the H-RIS is located a distance of $(x_t, 0)$ as shown in Figure 2 where, x_t and $x_{SUE,u}$ might vary.

Thus, the distance between the i^{th} SBS and the u^{th} SUE is $d_1 = \sqrt{(x_{SUE,u})^2 + (y_{SUE,u})^2}$, whereas the distances between the i^{th} SBS and the H-RIS and the H-RIS and the u^{th} SUE are $d_t = x_t$ and $d_R = \sqrt{(d_t - x_{SUE,u})^2 + (y_{SUE,u})^2}$, respectively. The MBS is located at coordinates (300,0). Figure 2 demonstrates the simulation setup. The macro cell and the small cell have coverage radiuses of 500m and 20m [17], respectively.

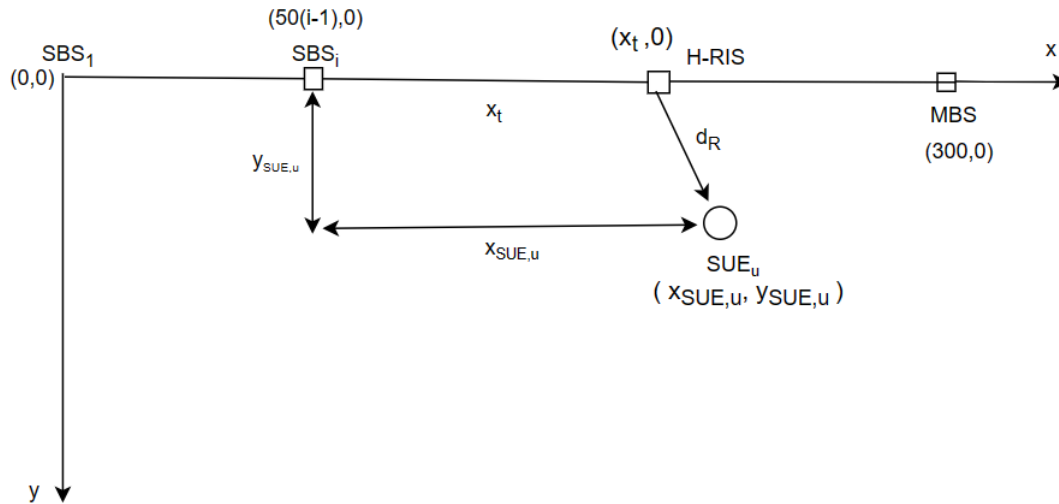


Figure 2. Simulation setup

At a distance d , the path loss of a link is given by [14], [15], [20].

$$\beta(d) = \beta_0 \left(\frac{d}{1m} \right)^{-\gamma} \quad (38)$$

Where, β_0 is the path loss at the reference distance of 1m, and γ is the path loss exponent. We adopt the Rician fading channel model for small-scale fading [14], [21]. The small-scale fading channel from the SBS to the H-RIS can therefore be described as [14], [21].

$$\bar{H} = \left(\sqrt{\frac{k}{1+k}} H^{LOS} + \sqrt{\frac{1}{1+k}} H^{NLOS} \right) \quad (39)$$

Where H^{LOS} and H^{NLOS} are the LOS and NLOS components, respectively, and k is the Rician factor. The non-line-of-sight (NLOS) channel is modeled by the rayleigh fading, being given as $h^{NLOS} \sim \mathcal{CN}(0, 1)$. The LOS components are produced by $e^{j\frac{2\pi}{\eta}(d)}$, where η is the wavelength. The method used to obtain the channel between the i^{th} SBS and the H-RIS is $H = \sqrt{\beta(d_t)} \bar{H}$. Those between H-RIS and the u^{th} SUE and the SBS and the u^{th} SUE are modeled similarly. We assume that the u^{th} SUE and the H-RIS are deployed at a distance of $(x_{SUE,u}, y_{SUE,u}) = (15, 5)m$, where $x_{SUE,u} = (65 - 50)m$ and $(70 - 50, 0) = (20, 0)m$, where $x_t = 20m$ respectively. The i^{th} SBS is deployed at $(50, 0)m$ from the origin. Table 1 display the specific parameter settings.

Table 1. System parameters

Parameters	Values
ϵ	10^{-8}
M	8
U	4
I	4
P_m	43 dBm [17]
P_{SBS}	300 mW [15]
$P_{SUE,u}$	200 mW [15]
P_b	2 mW [14, 15, 20]
P_{SW}	5 mW [15]
P_{max}^{RIS}	5 dBm [21]
P_i	25 dBm [17]
P_a	10 mW [15]
τ	0.45 [28]
β_0	-30 dB [14]
γ	3 [21]
$\sigma_r = \sigma_u$	-100 dBm [21]
k	4 [21]
Frequency	5 Ghz [21]

7. RESULTS AND DISCUSSION

Now, in order to evaluate the performance of the proposed H-RIS-assisted HetNet scheme, we compare its SE and EE with respect to the following benchmark schemes:

- No-RIS: in this instance, we set the phase shift matrix of the H-RIS to be zero. Therefore, in the signal that the u^{th} SUE has received, only the direct propagation path is considered.
- Passive RIS: in this case, we reduce the number of active elements to zero and set $[B]_N^Q = 0$, then optimise ϕ according to method (1) in section 4.
- Active RIS: in this scenario, we set the number of passive elements to zero and set $[B]_N^Q = 1$, then optimise ψ according to method (2) in section 4.

When $\alpha_n = 4$, Figure 3 demonstrates the SE in relation to N, the proposed scheme’s number of H-RIS elements, and three other benchmarks. Figure 3 demonstrates that for all the investigated values of N, the proposed AO-PMC scheme performs much better than both passive RIS optimised via AO [17] and active RIS-assisted HetNet optimised via AO [21] When there is no RIS in the network, it is different. This is due to the possibility that the no-RIS scheme will not contribute to the reduction of interference signals. The SE of the proposed H-RIS-assisted HetNet, passive and active RIS-assisted HetNet, also grows as the number of H-RIS elements increases, and the SE of H-RIS-assisted HetNet increases a little bit more quickly. In the case of the proposed AO-PMC scheme, the SE is 39, 67% greater than that of passive RIS-assisted HetNet optimised via AO when N = 50. As a result, it can be said that H-RIS-assisted HetNet performs better at interference reduction.

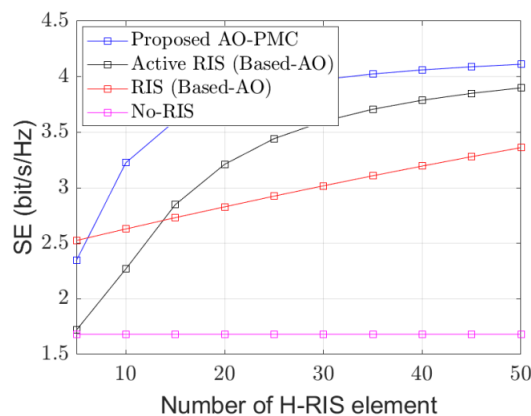


Figure 3. SE vs. the number of H-RIS elements N

The best RIS placement is then shown in Figure 4, where we show the SE of RIS for various passive/active RIS and H-RIS sites by adjusting d_t for $N=50$, $K=4$, and $\alpha_n=4$. Figure 4 demonstrates that the SE of RIS-related schemes initially shows a pattern of growth with regards to d_t , varying from 5 to 20, outperforming that without RIS (No-RIS), which performs much worse while remaining constant with d_t . In particular, the RIS loses the reflecting gains and performs almost as well as the scheme without the RIS when it moves away from both the SBS and the SUE for $d_t \geq 15m$. The suggested AO-PMC scheme, in contrast, shows significant performance increases over both passive and active RIS-based AO schemes.

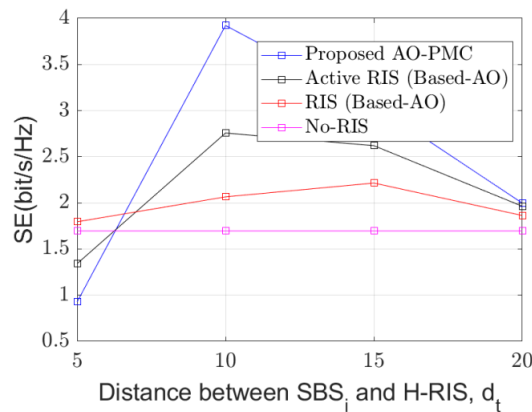


Figure 4. SE with respect to different positions of the H-RIS-assisted HetNet

For the H-RIS-assisted HetNet with $N=64$ and $K=4$, we demonstrate the SE performance improvement in Figure 5. As a result, for all possible values of α_n , the AO-PMC scheme performs better than the passive RIS based-AO scheme with N completely passive reflecting elements. For instance, the SE of the proposed AO-PMC scheme aided system with $\alpha_n=2$ rises by 19, 87% at a transmit power of 15 dBm. In addition, the proposed AO-PMC scheme and the active RIS-assisted system-based AO scheme improve the system's performance under various α_n . This suggests that, even with a small P_i , the proposed AO-PMC scheme can achieve better performance. It is interesting to note that the proposed AO-PMC scheme produces roughly the same results at $\alpha_n=2$ as it does at $\alpha_n=4$ for the active RIS-based AO scheme. This is a result of active elements adding extra amplification noise. As a result, the amplification factors of active RIS with N fully active elements cannot be too low in order to counteract the high noise.

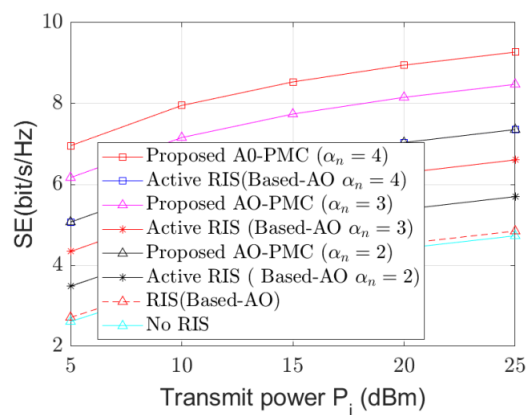


Figure 5. SE with respect to the transmit power

When $N=96$, $K=2$, $d_t=30m$ and $x_{SUE,u}=35m$ are used, Figure 6 demonstrates the SE versus the number of antennas at the MBS for the proposed AO-PMC scheme and benchmark schemes. AO-PMC, active RIS-based AO, passive RIS-based AO, and no-RIS are permutations of all schemes in decreasing order of SE,

much like in Figure 5. The figure shows that, despite a rise in α_n , the SE of the eight schemes reduces as the number of antennas at the MBS grows. Both the proposed AO-PMC scheme and the active RIS-based AO scheme perform similarly when M is small and $\alpha_n = 2$ and 4, respectively, but as M increases, the performance differences between the two schemes becomes larger. According to the curves in Figure 6, in particular, the SE gap between the proposed AO-PMC and others schemes widens at first before closing, reflecting the fact that the SE of the proposed AO-PMC scheme decreases with M at a slower rate than that of the passive RIS-assisted HetNet based-AO and conventional HetNet (No-RIS). Therefore, it can be said that the H-RIS-assisted HetNet based AO-PMC performs better in terms of blocking cross and co-tier interference.

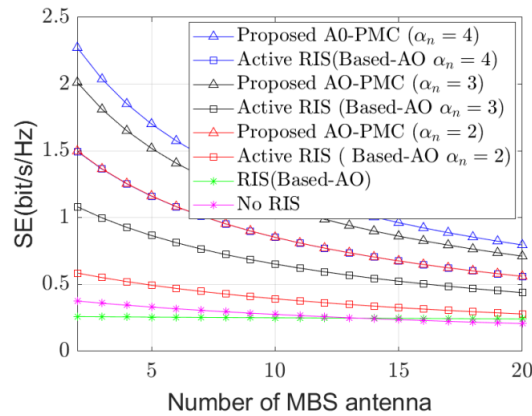


Figure 6. SE vs. the number of antennas at the MBS, M

Figure 7 demonstrates the proposed H-RIS-based AO-PMC’s EE performance enhancement for a 1×1 SISO system. Passive RIS-based AO, active RIS-based AO, and AO-PMC all have $N = 50$ elements, $M = N - K = 48$, and $\alpha_n = 4$. It is demonstrated that the proposed AO-PMC schemes outperform the active RIS-based AO scheme in terms of EE, particularly at low and intermediate P_i , and are comparable to the passive RIS-based AO scheme as well as the SISO (No-RIS) scheme. This explains why H-RIS can achieve a bigger performance gain with restricted P_i .

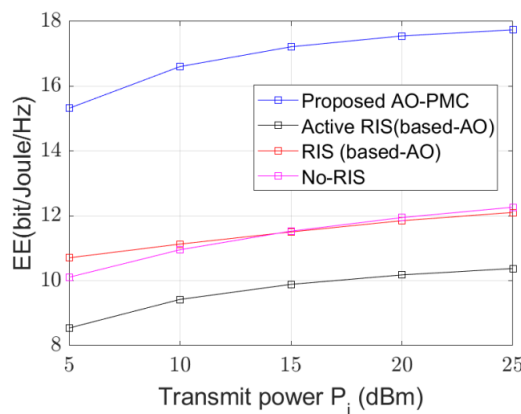


Figure 7. EE performance

The EE for various physical RIS and H-RIS sizes is demonstrated in Figure 8. In particular, for a 1×1 SISO system, we set $K = 2$, $N = [5, 50]$, and $\alpha_n \in [2, 3, 4]$. When compared to the passive RIS-based AO and active RIS-based AO, respectively, the proposed AO-PMC schemes are demonstrated to significantly outperform both for all relevant values of N and α_n . We observed that for the active RIS-based AO scheme, when N rises, the EE falls even as α_n rises. This is due to the active use of electricity by the active RIS elements, which results in a very high-power consumption from the active RIS.

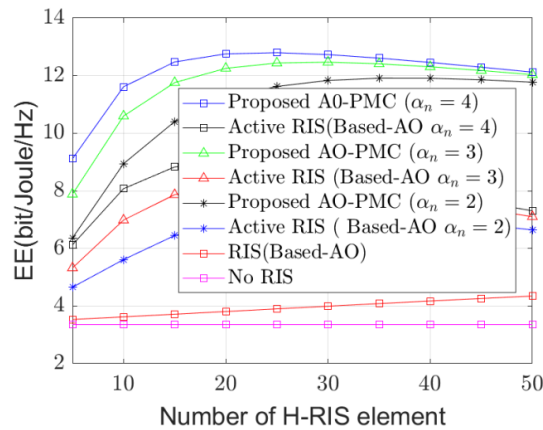


Figure 8. EE performance for $N = [5, 50]$

We demonstrate the convergence of the proposed AO-PMC scheme in Figure 9, when $N = 50$ and $K = 4$. It is found that the suggested AO-PMC scheme has good convergence since for all value of α_n , a maximum of six iterations are required for convergence.

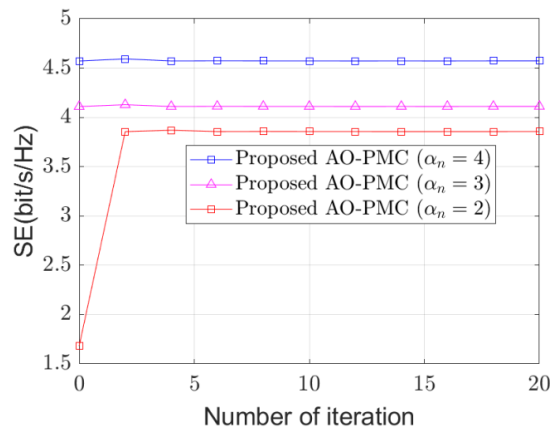


Figure 9. Convergence of the proposed algorithm

8. CONCLUSION

The implementation of hybrid RIS in HetNet communication systems was our suggestion. A small number of active elements were used in this hybrid RIS to give it reflecting and amplifying advantages. In order to optimise the RIS amplifying and reflecting coefficients, we formulated a rate maximisation problem and proposed an effective AO-PMC method. Finally, comprehensive numerical results were used to evaluate the proposed design. The incorporation of hybrid RIS into HetNet was mathematically demonstrated to have the ability to significantly minimise interference by turning all interference channels to zeros. Additionally, even when the amplification factor is not large, the hybrid RIS-assisted HetNet performs better in terms of interference control than HetNet without RIS, passive RIS-assisted HetNet schemes, and active RIS-assisted HetNet schemes. Using the advantage of model-based optimisation, this work mainly focuses on AO-based methods for spectrum and energy-efficient H-RIS-assisted interference reduction for HetNet systems. However, we recognise that by utilising their adaptive qualities and capacity to capture intricate system dynamics, machine learning and metaheuristics techniques have the potential to further improve our solutions. In order to improve the energy efficiency of H-RIS-assisted HetNet, future research will examine the sophisticated ML and metaheuristic approaches and take into account their integration with model-based algorithms.

ACKNOWLEDGMENTS

This work is supported by the African Union (AU).




REFERENCES

- [1] C. Huang, A. Zappone, G. C. Alexandropoulos, M. Debbah, and C. Yuen, "Reconfigurable intelligent surfaces for energy efficiency in wireless communication," *IEEE Transactions on Wireless Communications*, vol. 18, no. 8, pp. 4157–4170, Aug. 2019, doi: 10.1109/TWC.2019.2922609.
- [2] R. Fara, P. Ratajczak, D.-T. Phan-Huy, A. Ourir, M. Di Renzo, and J. De Rosny, "A prototype of reconfigurable intelligent surface with continuous control of the reflection phase modeling, full-wave electromagnetic characterization, experimental validation, and application to ambient backscatter communications," *IEEE Wireless Communications*, vol. 29, no. 1, pp. 70–77, 2022.
- [3] W. Mei, B. Zheng, C. You, and R. Zhang, "Intelligent reflecting surface aided wireless networks: from single-reflection to multi-reflection design and optimization," *Arxiv*, 2021.
- [4] E. Björnson and L. Marcenaro, "Configuring an intelligent reflecting surface for wireless communications: highlights from the 2021 IEEE Signal Processing Cup student competition [SP Competitions]," *IEEE Signal Processing Magazine*, vol. 39, no. 1, pp. 126–131, Jan. 2022, doi: 10.1109/MSP.2021.3123593.
- [5] A. N. Soumana Hamadou, C. wa Maina, and M. M. Soidridine, "Cross-tier interference mitigation for RIS-assisted heterogeneous networks," *Technologies*, vol. 11, no. 3, p. 73, 2023, doi: 10.3390/technologies11030073.
- [6] A. Nasser Soumana Hamadou, S. Member, C. wa Maina, and M. Moindze Soidridine, "Hybrid RIS-assisted Interference mitigation for heterogeneous networks," *Authorea Preprints*, 2023, [Online]. Available: <https://doi.org/10.36227/techrxiv.24083586.v1>.
- [7] J. An, C. Xu, L. Gan, and L. Hanzo, "Low-complexity channel estimation and passive beamforming for RIS-assisted MIMO systems relying on discrete phase shifts," *IEEE Transactions on Communications*, vol. 70, no. 2, pp. 1245–1260, Feb. 2022, doi: 10.1109/TCOMM.2021.3127924.
- [8] D. Xu, X. Yu, Y. Sun, D. W. K. Ng, and R. Schober, "Resource allocation for IRS-assisted full-duplex cognitive radio systems," *IEEE Transactions on Communications*, vol. 68, no. 12, pp. 7376–7394, Dec. 2020, doi: 10.1109/TCOMM.2020.3020838.
- [9] S. Jiao, X. Xie, and Z. Ding, "Deep reinforcement learning-based optimization for RIS-based UAV-NOMA downlink networks (invited paper)," *Frontiers in Signal Processing*, vol. 2, Jul. 2022, doi: 10.3389/frsip.2022.915567.
- [10] A. Mondal, A. M. H. Al Junaedi, K. Singh, and S. Biswas, "Spectrum and energy-efficiency maximization in RIS-aided IoT networks," *IEEE Access*, vol. 10, pp. 103538–103551, 2022, doi: 10.1109/ACCESS.2022.3209823.
- [11] J. Wang, S. Wang, S. Han, and C. Li, "Intelligent reflecting surface secure backscatter communication without eavesdropping CSI," *IEEE Communications Letters*, vol. 27, no. 6, pp. 1496–1500, Jun. 2023, doi: 10.1109/LCOMM.2023.3267093.
- [12] Y. Xu *et al.*, "Robust resource allocation for two-tier HetNets: an interference-efficiency perspective," *IEEE Transactions on Green Communications and Networking*, vol. 5, no. 3, pp. 1514–1528, Sep. 2021, doi: 10.1109/TGCN.2021.3090592.
- [13] M. Osama, S. El Ramly, and B. Abdelhamid, "Interference mitigation and power minimization in 5G heterogeneous networks," *Electronics (Switzerland)*, vol. 10, no. 14, p. 1723, Jul. 2021, doi: 10.3390/electronics10141723.
- [14] N. T. Nguyen, Q. D. Vu, K. Lee, and M. Juntti, "Hybrid relay-reflecting intelligent surface-assisted wireless communications," *IEEE Transactions on Vehicular Technology*, vol. 71, no. 6, pp. 6228–6244, Jun. 2022, doi: 10.1109/TVT.2022.3158686.
- [15] J. C. Chen, "Capacity improvement for intelligent reflecting surface-assisted wireless systems with a small portion of active elements," *IEEE Access*, vol. 10, pp. 100438–100445, 2022, doi: 10.1109/ACCESS.2022.3207495.
- [16] F. Wang and A. L. Swindlehurst, "Hybrid ris-assisted interference mitigation for spectrum sharing," in *ICASSP, IEEE International Conference on Acoustics, Speech and Signal Processing - Proceedings*, Jun. 2023, pp. 1–5, doi: 10.1109/ICASSP49357.2023.10096639.
- [17] Y. XU *et al.*, "Resource allocation for two-tier RIS-assisted heterogeneous NOMA networks," *ZTE Communications*, vol. 20, no. 1, pp. 36–47, 2022, doi: 10.12142/ZTECOM.202201006.
- [18] W. Tan, Q. Zhou, W. Tan, L. Yang, and C. Li, "Performance analysis of intelligent reflecting surface assisted wireless communication system," *CMES - Computer Modeling in Engineering and Sciences*, vol. 137, no. 1, pp. 775–787, 2023, doi: 10.32604/cmescs.2023.027427.
- [19] Z. Zhu *et al.*, "Intelligent reflecting surface-assisted wireless powered heterogeneous networks," *IEEE Transactions on Wireless Communications*, vol. 22, no. 12, pp. 9881–9892, Dec. 2023, doi: 10.1109/TWC.2023.3274220.
- [20] S. Ao *et al.*, "Resource allocation for RIS-assisted device-to-device communications in heterogeneous cellular networks," *IEEE Transactions on Vehicular Technology*, vol. 72, no. 9, pp. 11741–11755, Sep. 2023, doi: 10.1109/TVT.2023.3267032.
- [21] Z. Zhang *et al.*, "Active RIS vs. Passive RIS: which will prevail in 6G?," *IEEE Transactions on Communications*, vol. 71, no. 3, pp. 1707–1725, Mar. 2023, doi: 10.1109/TCOMM.2022.3231893.
- [22] M. Xu, M. Mao, Y. Feng, T. Li, R. Shi, and Y. He, "Beamforming design for max-min SINR in RIS-based hybrid relaying," *IET Communications*, vol. 17, no. 10, pp. 1220–1227, Jun. 2023, doi: 10.1049/cmu2.12611.
- [23] Q. Wu and R. Zhang, "Intelligent reflecting surface enhanced wireless network via joint active and passive beamforming," *IEEE Transactions on Wireless Communications*, vol. 18, no. 11, pp. 5394–5409, Nov. 2019, doi: 10.1109/TWC.2019.2936025.
- [24] H. Niu and X. Liang, "Weighted sum-rate maximization for STAR-RISs-aided networks with coupled phase-shifters," *IEEE Systems Journal*, vol. 17, no. 1, pp. 1083–1086, Mar. 2023, doi: 10.1109/JSYST.2022.3159551.
- [25] M. Ahmed *et al.*, "A survey on STAR-RIS: use cases, recent advances, and future research challenges," *IEEE Internet of Things Journal*, vol. 10, no. 16, pp. 14689–14711, Aug. 2023, doi: 10.1109/JIOT.2023.3279357.
- [26] A. M. C. So, J. Zhang, and Y. Ye, "On approximating complex quadratic optimization problems via semidefinite programming relaxations," *Mathematical Programming*, vol. 110, no. 1, pp. 93–110, Mar. 2007, doi: 10.1007/s10107-006-0064-6.
- [27] E. Björnson, O. Ozdogan, and E. G. Larsson, "Intelligent reflecting surface versus decode-and-forward: how large surfaces are needed to beat relaying?," *IEEE Wireless Communications Letters*, vol. 9, no. 2, pp. 244–248, 2020, doi: 10.1109/LWC.2019.2950624.


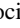
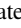
- [28] W. Dinkelbach, "On nonlinear fractional programming," *Management Science*, vol. 13, no. 7, pp. 492–498, Mar. 1967, doi: 10.1287/mnsc.13.7.492.
- [29] CVX Research, "CVX: Matlab software for disciplined convex programming — CVX Research, Inc.," *CVX Research, Inc.*, 2020. <http://cvxr.com/cvx/> (accessed May 20, 2023).
- [30] K. Shen and W. Yu, "Fractional programming for communication systems - part i: power control and beamforming," *IEEE Transactions on Signal Processing*, vol. 66, no. 10, pp. 2616–2630, May 2018, doi: 10.1109/TSP.2018.2812733.
- [31] E. Björnson, J. Hoydis, and L. Sanguinetti, "Massive MIMO networks: spectral, energy, and hardware efficiency," *Foundations and Trends in Signal Processing*, vol. 11, no. 3–4, pp. 154–655, 2017, doi: 10.1561/20000000093.

BIOGRAPHIES OF AUTHORS



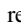


Abdel Nasser Soumana Hamadou    received the Graduate Engineer degree in Telecommunication (2018) and the M.Sc. degree in Radiocommunication and Services (2020), respectively, from the Ecole Supérieure Multinationale des Télécommunications (ESMT) in Dakar, Senegal. He is currently a Ph.D. student in Telecommunications at the Pan African University Institute for Basic Science, Technology, and Innovation (PAUSTI), Nairobi, Kenya. His research interests include 5G and beyond, interference management, reconfigurable intelligent surfaces, metaheuristic optimisation, and machine learning. He can be contacted at email: nasser.abdel@students.jkuat.ac.ke.



Ciira wa Maina    is an Associate Professor at Dedan Kimathi University of Technology (DeKUT) in Nyeri, Kenya. He teaches electrical engineering and also conducts research in a number of areas, including bioacoustics, IoT, machine learning, and data science. Since September 2019, he has led the Centre for Data Science and Artificial Intelligence (DSAIL). Prior to joining DeKUT in 2013, he was a postdoctoral researcher at the University of Sheffield between 2011 and 2013, a Ph.D. student at Drexel University in Philadelphia, USA, between 2007 and 2011, and a BSc. student at the University of Nairobi between 2002 and 2007. He can be contacted at email: ciira.maina@dkut.ac.ke.



Moussa Moindze Soidridine    received his Ph.D. in Computer Science at Cheikh Anta Diop University, Dakar, in 2018. He is currently a research professor at UAMA University, Dakar. He is also an expert in network security, cyber security, and AI/IoT. Dr. Moindze has published several articles, and his research interests are in network security, cyber security, AI/IoT, management and control of spectrum frequencies, optical network performance, management of emerging NGN/NGS, and cellular and mobile networks (3G, 4G, 5G, and 6G) dimensioning, planning, and QoS/QoE optimization. He can be contacted at email: smoindze1@gmail.com.